Robust High-Speed Train Handover Optimization Using Velocity-Adaptive Fuzzy Logic in 5G/B5G Networks

Liku Kimola Chenge
Department of Electrical Engineering, Pan African University Institute for Basic Sciences and Technology and Innovation (PAUISTI), Kiambu, Kenya
chengeliku@gmail.com (corresponding author)

Clement Temaneh Nyah
Department of Electrical and Computer Engineering, University of Namibia, Windhoek, Namibia
clementtemaneh@yahoo.com

Edwin O. Ataro
Department of Electrical and Communications Engineering, Moi University, Eldoret, Kenya
ataro@mu.ac.ke

Received: 24 February 2026 | Revised: 2 April 2026 | Accepted: 17 April 2026

 DOI: https://doi.org/10.48084/etasr.18362

ABSTRACT

Efficient communication in High-Speed Trains (HSTs) is a crucial factor in maintaining reliable, safe, and continuous railway operations. However, high speed affects the handover process to a large extent, leading to interrupted communication services due to the rapid crossing of adjacent cells and variations in the radio channel. This problem is more pronounced in fifth-generation (5G) and Beyond 5G (B5G) networks, where the dense deployment of cells increases the Handover Rates (HORs). Traditional Event A3-based algorithms rely on fixed Handover Control Parameters (HCPs) that are unable to adapt to rapidly deteriorating link quality and increasingly unstable wireless channels as the train speed increases. Therefore, in this study, we propose a Velocity-Adaptive Dual-Segment Fuzzy Logic Controller (VADFLC) that can adjust the HCPs based on the Reference Signal Received Power (RSRP) and speed of the User Equipment (UE). The approach is implemented in a MATLAB simulation tool and validated against the Traditional A3 algorithm. The results show that the proposed method reduces the HOR by approximately 25.5% compared to the Traditional A3 algorithm, significantly lowers the Handover Ping-Pong (HOPP) ratio by up to 95%, and improves Handover Delay (HOD) behavior, with the delay decreasing by approximately 33% as the UE speed increases. In addition, an average delay reduction of approximately 1.0% is achieved under a different 5G for Railways (5G-R) simulation setup.

Keywords-5G NR; fuzzy logic controller; handover optimization; high-speed train communications; mobility robustness optimization

I. INTRODUCTION

The transition towards modern transportation systems, such as High-Speed Trains (HSTs), requires high-quality services to ensure seamless communication [1]. Because fifth-generation (5G) and Beyond 5G (B5G) wireless networks are characterized by ultra-high data rates, ultra-low latency, and massive connectivity [2], the adoption of 5G for Railways (5G-R) technology, which proves to be the most promising solution for HST communication, has been suggested [3]. In addition, 5G/B5G networks operate under high frequencies ranging from Frequency Range 1 (sub-6 GHz) to millimeter-wave (mmWave) bands, which causes rapid signal attenuation and poor obstacle penetration [4]. Network operators deploy dense small cells to maintain coverage and capacity [5]. Although the dense deployment of Base Stations (BSs) increases capacity and spectral efficiency, it also increases the handover frequency, which presents a major challenge for handover process management [6]. This situation becomes more severe in ultra-high-mobility scenarios, where a reduced cell residence time constrains reliable handover execution [7, 8]. Field-measurement analysis of an operational Long-Term Evolution (LTE) network reported in [9] further demonstrated that increasing User Equipment (UE) speed (80–140 km/h) significantly increases handover preparation time and handover

failure probability, leading to degraded seamless connectivity in highway scenarios.

Recently, most Internet Service Providers (ISPs) have opted to deploy 5G outdoor BSs to facilitate reliable, seamless, and high-quality communication services. To achieve such performance, optimal tuning of Handover Control Parameters (HCPs) is required to ensure timely and reliable handover execution as the UE moves across cell edges [5]. The 3rd Generation Partnership Project (3GPP) Radio Resource Control (RRC) specifies four HCPs for 5G: Time-to-Trigger (TTT), hysteresis margin (Hys), offset (such as A3 Offset for Event A3 handover (HO) triggering condition), and signal level threshold, and establishes six measurement events (handover triggering conditions) to determine when a handover should occur. These events can be classified as either relative triggering conditions (in which the serving cell measurements are directly compared to the target cell measurements) or absolute triggering conditions (in which the serving cell or the target cell measurements are compared against the threshold), as illustrated in Table I [10].

TABLE I. SUMMARY OF HANDOVER MEASUREMENT EVENTS

Handover measurement event	Condition	Relative	Absolute
Event A1	$RSRP_{serving} > RSRP_{threshold} + Hys$ The serving cell becomes better than the threshold		✓
Event A2	$RSRP_{serving} < RSRP_{threshold} - Hys$ The serving cell becomes worse than the threshold		✓
Event A3	$RSRP_{target} > RSRP_{serving} + A3\ Offset + Hys$ The target cell becomes better than that of the primary serving cell (PCell) by a specified offset	✓	
Event A4	$RSRP_{target} > RSRP_{threshold} + Hys$ The target cell becomes better than threshold		✓
Event A5	$RSRP_{serving} < RSRP_{threshold1} - Hys$ & $RSRP_{target} > RSRP_{threshold2} + Hys$ The serving cell becomes worse than threshold 1 and target cell becomes better than threshold 2		✓
Event A6	$RSRP_{target} > RSRP_{secondary} + Offset + Hys$ The target cell becomes offset better than the secondary serving cell	✓	

RSRP: Reference Signal Received Power.

Among these events, Event A3 is one of the most widely used conditions [10]. As depicted in Figure 1, this is a relative condition, which specifies that a handover is triggered only if the target cell measurement result becomes better than that of the primary serving cell (PCell) by a specified offset. This condition is continuously satisfied for a predefined amount of time, known as the TTT, which is crucial in preventing unnecessary handovers resulting from transient signal peaks caused by fast fading and shadowing effects.

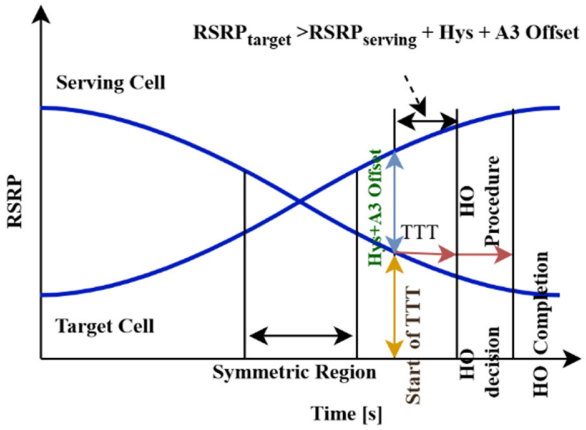

Fig. 1. Event A3 HO procedure.

The traditional Event A3-based HO algorithm, referred to as Traditional A3, operates with fixed HCPs [11]. In common operational practice, HCPs are configured using vendor-defined defaults or by performing manual tuning based on expert experience through multiple trials. Although these practices provide practical results in static environments, they are time-consuming and suboptimal when applied to dynamic environments [12]. The main limitation of the Traditional A3 algorithm is its one-size-fits-all approach, which fails to adapt to variations in user mobility and wireless channel conditions. This lack of adaptability affects the Quality of Service (QoS) across different mobility scenarios. For example, a UE moving at low-speed benefits from a longer, more stable handover process that avoids rapid, back-and-forth handovers (ping-pong) between cells. In contrast, a fixed TTT that is too short can trigger premature handover events, generating excessive signaling overhead and inefficient consumption of network resources. In contrast, a UE moving at a high speed, such as in HST scenarios, requires rapid handover execution. A fixed TTT that is too long can delay the handover process, causing the user to cross the cell boundary before the handover is completed. This delay leads to excessive Handover Delays (HODs), which increase the risk of Handover Failures (HOFs) and Radio Link Failures (RLFs), ultimately degrading overall service quality.

Thus, the Traditional A3 algorithm fails to perform efficiently in fast-changing environments because it cannot dynamically balance the competing needs of handover stability and responsiveness, making it suboptimal for environments where user speed and channel conditions vary rapidly [13, 14]. This demonstrates the urgent need for a self-optimizing handover algorithm that is intelligent and capable of dynamically tuning HCPs in real time.

Several studies have developed handover optimization schemes to enhance mobility robustness in LTE, 5G, and B5G networks. Authors in [15] proposed a fuzzy multi-criteria

decision-making method based on TOPSIS to improve target cell selection for dense LTE macrocells. In [11, 14], the limitations of the handover parameter configurations by static selection were addressed; however, both approaches were limited to LTE networks. In [16-18], fuzzy logic-based handover optimization schemes were proposed. Considering the significant influence of the UE speed on handover performance, authors in [19] introduced velocity awareness into the handover self-optimization. In [7, 20], mobility management in high-speed scenarios for 5G-R was investigated. On the other hand, authors in [21, 22] proposed machine learning-based techniques for designing adaptive handover methods.

Although existing studies have demonstrated improvements in HCPs optimization, they still suffer from the following key gaps:

- Focusing on static HCPs or optimizing only a subset of parameters, typically Hys and TTT, neglects dynamic A3 Offset optimization.
- They are primarily validated in urban or ultra-dense small-cell environments under low UE mobility and therefore lack applicability to ultra-high-mobility 5G macrocell networks, particularly in HST scenarios.

This study proposes a Velocity-Adaptive Dual-Segment Fuzzy Logic Controller (VADFLC) framework for ultra-high-mobility 5G/B5G handovers to address these limitations. The proposed controller dynamically tunes the A3 Offset, hysteresis margin, and TTT in real time based on the UE velocity and Reference Signal Received Power (RSRP), thereby enabling efficient and robust handover operation for HST communications.

II. METHODOLOGY

Figure 2 presents an overview of the proposed methodology for addressing handover optimization and mobility management challenges in ultra-high-mobility 5G macrocell networks. The proposed methodology consists of three steps that begin with the development of a system and channel model. This is followed by the design and integration of a VADFLC into the system and channel model developed to achieve adaptive handover control. Finally, the complete VADFLC framework obtained after integrating the VADFLC into the developed system model was implemented and evaluated on a MATLAB platform to analyze its performance in ultra-high-speed scenarios.

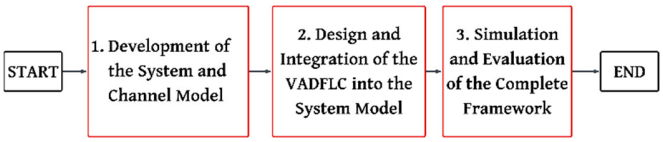

Fig. 2. Proposed methodology overview.

A. System and Channel Model

In this study, we considered a Rural Macrocell (RMa) deployment that complies with the specifications of 3GPP TR 38.901. Hence, all physical-layer and propagation parameters follow the sub-6 GHz channel modeling guidelines for RMa environments defined in 3GPP TR 38.901 [4]. The objective was to characterize the RSRP experienced by a HST operating at a carrier frequency $f_c = 3.5$ GHz. The cellular layout follows a regular hexagonal grid with an inter-site distance D of 5 km. Each site (gNodeB) comprises three 120° sectors, each equipped with a single transmit antenna. The UE, representing the HST, is equipped with a single omnidirectional antenna. The BS and UE antenna heights were $h_{BS} = 35$ m and $h_{UE} = 3$ m, respectively. As illustrated in Figure 3, the train moves along a straight predefined railway trajectory with velocity $v \in [100, 400]$ km/h.

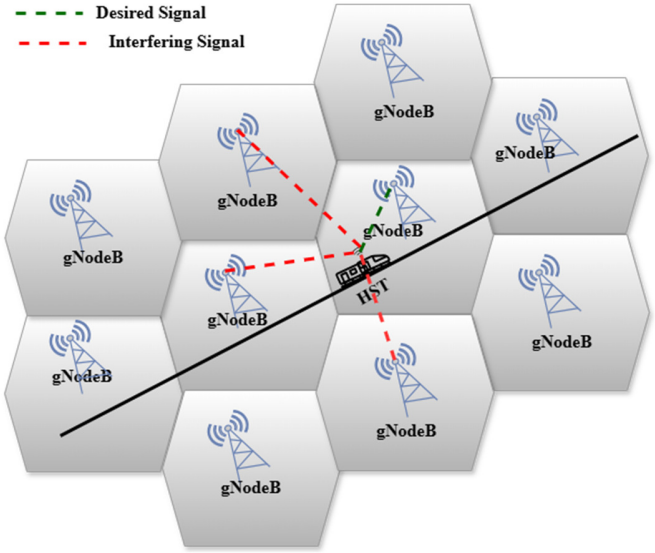

Fig. 3. System model of the considered 5G RMa network and UE mobility.

The UE motion was modeled as deterministic linear mobility, which is suitable for railway scenarios. The three-dimensional position vector $p_{UE}(t)$ of the UE at time t is expressed as follows:

$$p_{UE}(t) = \begin{bmatrix} x_{UE}(t) \\ y_{UE}(t) \\ h_{UE} \end{bmatrix} \quad (1)$$

To simplify the analysis in this study, the UE was assumed to move with a constant velocity vector v_{UE} given by $v_{UE} = \begin{bmatrix} v_x \\ v_y \end{bmatrix}$. The UE radial velocity component v was then obtained as $v = \sqrt{v_x^2 + v_y^2}$. The UE position $[x_{UE}, y_{UE}]$ was updated according to a linear kinematic model, as expressed in (2) and (3):

$$x_{UE}(t + \Delta t) = x_{UE}(t) + v_x \Delta t \quad (2)$$

$$y_{UE}(t + \Delta t) = y_{UE}(t) + v_y \Delta t \quad (3)$$

where Δt denotes the simulation time step, $x_{UE}(t)$ represents the horizontal coordinate of the UE along the x-axis (in meters) at time t, and $y_{UE}(t)$ is the horizontal coordinate of the UE

along the y-axis (in meters) at time t. This mobility formulation is particularly suitable for modeling HST scenarios, in which abrupt changes in speed are minimal.

At time t, the horizontal distance $d_{2D}^{(i)}(t)$ between the UE and the serving i^{th} BS yields a three-dimensional separation distance $d_{3D}^{(i)}(t)$, which was computed as follows:

$$d_{3D}^{(i)}(t) = \sqrt{\left(d_{2D}^{(i)}(t)\right)^2 + (h_{BS} - h_{UE})^2} \quad (4)$$

where $d_{2D}^{(i)}(t) = \sqrt{\left(x_{BS}^{(i)} - x_{UE}(t)\right)^2 + \left(y_{BS}^{(i)} - y_{UE}(t)\right)^2}$.

For each gNodeB, the serving sector was selected according to the maximum antenna gain towards the UE. The sector antenna pattern follows the standard 3GPP TR 38.901 directional model [4]. The horizontal attenuation $A_H(\phi)$ was obtained as follows:

$$A_H(\phi) = -\min\left(12\left(\frac{\phi}{\phi_{3dB}}\right)^2, A_m\right) \quad (5)$$

where ϕ denotes the azimuth offset from the sector boresight, $\phi_{3dB} = 65°$ represents the half-power (3 dB) beamwidth of the sector antenna in the horizontal plane, and $A_m = 30$ dB denotes the maximum horizontal attenuation of the sector antenna pattern. The corresponding sector gain $G(\phi)$ towards the UE is expressed as:

$$G(\phi) = G_{max} + A_H(\phi) \quad (6)$$

with maximum antenna gain $G_{max} \approx 15–18$ dBi. The UE antenna gain G_{UE} was assumed as $G_{UE} \approx 0$ dBi.

In this study, we adopted the Close-In (CI) path-loss model [23] and set parameters consistent with 3GPP TR 38.901. The CI path-loss model with a reference distance of 1 m expresses the large-scale path loss (in decibels) $PL\left(d_{3D}^{(i)}(t)\right)$ between the UE and serving BS at time t, as given in (7):

$$PL\left(d_{3D}^{(i)}(t)\right) = FSPL(1\,m) + 10n\log_{10}\left(d_{3D}^{(i)}(t)\right) + X_\sigma \quad (7)$$

where:

$$FSPL(1\,m) = 20\log_{10}\left(\frac{c}{4\pi f_c}\right) \quad (8)$$

At $f_c = 3.5$ GHz and with the speed of light in free space $c = 3 \times 10^8$ m/s, the free-space path loss at 1 m is $FSPL(1\,m) = 43.28$ dB. The path-loss exponent was set to $n = 2.1$ for Line-of-Sight (LoS) and $n = 3.0$ for Non-Line-of-Sight (NLoS) conditions to characterize signal attenuation with distance. Shadow fading X_σ was modeled as $X_\sigma \sim \mathcal{N}(0, \sigma^2)$, with standard deviations of $\sigma = 4$ dB (LoS) and $\sigma = 8$ dB (NLoS).

The LoS probability $P_{LoS}(d)$ for the RMa scenario is computed by:

$$P_{LoS}(d) = \begin{cases} 1, & d_{2D}^{(i)}(t) \le 10m \\ e^{\left(-\frac{d_{2D}^{(i)}(t)-10}{1000}\right)}, & d_{2D}^{(i)}(t) > 10m \end{cases} \quad (9)$$

Accordingly, the propagation state is determined probabilistically based on the horizontal distance $d_{2D}^{(i)}(t)$. Under these assumptions, the RSRP at time t (in dBm) is computed as follows:

$$RSRP(t) = P_{tx} + G(\phi(t)) - PL\left(d_{3D}^{(i)}(t)\right) + G_{UE} \quad (10)$$

where P_{tx} denotes the per-sector transmit power in dBm, $G(\phi(t))$ is the sector antenna gain (in dBi) towards the UE at time t, and G_{UE} represents the UE antenna gain (in dBi). Because RSRP represents an average over reference signal elements, fast fading was not explicitly modeled.

Finally, high train speeds introduce Doppler shifts characterized by:

$$f_D = \frac{v}{c} f_c \quad (11)$$

where f_D represents the maximum Doppler frequency shift (in Hz). Although Doppler affects instantaneous channel variations, its impact on RSRP is mitigated through measurement averaging.

The developed system and channel model captures the rapidly changing nature of RSRP variations due to the high UE speed and varying signal propagation conditions along the railway track. These RSRP variations directly impact the handover triggering behavior and highlight the constraints of fixed HCP configurations in ultra-high-mobility scenarios, such as HSTs. To address the effects of UE speed and radio propagation condition variations, an adaptive and velocity-aware handover control approach is required.

B. Velocity-Adaptive Dual-Segment Fuzzy Logic Controller Design and Integration

Figure 4 illustrates the closed-loop integration of the designed VADFLC into a 5G RMa system and channel model. The VADFLC dynamically tunes three key HCPs (A3 Offset, Hys, and TTT) based on real-time changes in the UE speed and channel conditions (specifically, RSRP) to improve the handover decision and mobility robustness in ultra-high-mobility 5G RMa networks.

The designed VADFLC comprises two modular Mamdani-type Fuzzy Inference Systems (FISs), each of which performs a specific optimization task. The first fuzzy logic controller (FLC 1) adaptively tunes the A3 Offset and Hys parameters to control the neighbor cell dominance relative to the serving cell, balancing the contributions from the UE speed and RSRP.

The second fuzzy logic controller (FLC 2) independently optimizes the TTT parameter with a velocity-adaptive focus to enforce a smooth inverse relationship between the UE speed and TTT. Longer TTTs improve performance at low speeds, whereas shorter TTTs prevent delayed handovers and consequently reduce HOD at high speeds.

In both FLC 1 and FLC 2, three important fuzzy logic processes were considered: fuzzification, inference mechanism, and defuzzification.

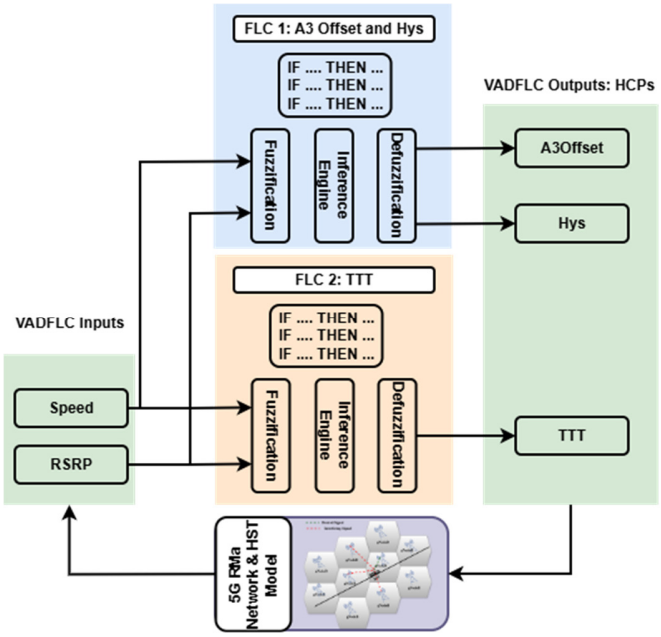

Fig. 4. Closed-loop integration of VADFLC into the 5G RMa system and channel model.

1) Fuzzification

In this study, we considered two inputs in the fuzzification stage: UE speed and RSRP. These two inputs were chosen because of their direct physical correlation with cell residence time and link quality. Speed represents the temporal aspect of UE mobility, and RSRP reflects the current signal strength of the serving cell.

Triangular membership functions defined in (12) [24] were adopted for all variables because of their low computational complexity and ability to provide smooth parameter transitions:

$$\mu(x) = \begin{cases} 0, & x \le a \text{ or } x \ge c \\ \frac{x-a}{b-a}, & a < x \le b \\ \frac{c-x}{c-b}, & b < x < c \end{cases} \quad (12)$$

where a, b, and c denote the left, peak, and right points of the triangle, respectively; x represents the variable in the domain (the universe of discourse); $\mu(x)$ denotes the membership value of x in the fuzzy set, representing the degree to which x belongs to the set, usually satisfying $\mu(x) \in [0,1]$.

As illustrated in Figures 5(a) and 5(e), RSRP was characterized using five linguistic sets defined within practical 5G New Radio (NR) operating ranges: VeryWeak (−130 to −100 dBm), Weak (−115 to −85 dBm), Medium (−100 to −70 dBm), Strong (−85 to −55 dBm), and VeryStrong (−70 to −40 dBm). The same RSRP classification was consistently applied in both FLC 1 and FLC 2.

For UE speed in FLC 1, three linguistic sets were used, as shown in Figure 5(b): Low (0–200 km/h), Medium (0–400 km/h), and High (200–400 km/h). In contrast, FLC 2 employs a finer speed granularity to enforce a smooth inverse relationship between UE speed and TTT. As illustrated in Figure 5(f), five speed sets were defined: VeryLow (0–100 km/h), Low (0–200 km/h), Medium (100–300 km/h), High (200–400 km/h), and VeryHigh (300–400 km/h).

Note that all linguistic output variables (A3 Offset, Hys, and TTT) in Figure 5 are defined over bounded universes of discourse derived from standardized 5G operating ranges recommended by 3GPP RRC [10]. Moreover, the proposed membership functions of input and output variables were designed to sufficiently overlap to enable smooth changes in parameter values.

This design preserves good sensitivity to variations in UE speed and signal strength, resulting in a smooth handover adaptation across cell edges and speed transitions.

2) Inference Mechanism and Defuzzification

The fuzzified inputs were processed by two independent Mamdani inference engines corresponding to FLC 1 and FLC 2, producing the output parameters: A3 Offset, Hys, and TTT. For FLC 1, five linguistic sets were defined for the A3 Offset output, as shown in Figure 5(c): Negative (−14 to −10 dB), SlightlyNegative (−14 to −6 dB), Zero (−10 to −2 dB), SlightlyPositive (−6 to 2 dB), and Positive (−2 to 2 dB).

Similarly, the Hys output in FLC 1 was described by five sets, as illustrated in Figure 5(d): VerySmall (0–3.75 dB), Small (0–7.5 dB), Medium (3.75–11.25 dB), Large (7.5–15 dB), and VeryLarge (11.25–15 dB). The TTT output of FLC 2 was represented by five membership functions, as shown in Figure 5(g): VeryShort (60–80 ms), Short (60–100 ms), Medium (80–120 ms), Long (100–140 ms), and VeryLong (120–140 ms).

A total of twenty-five Mamdani IF–THEN rules were formulated, comprising 14 rules for FLC 1 and 11 rules for FLC 2, with the rule count determined by the combinations of input states. The FLC 1 rule base (Table II) jointly maps UE speed and serving-cell RSRP to A3 Offset and hysteresis margin, enabling coordinated control of the handover triggering threshold and stability margin. At low speeds and strong signal conditions, conservative A3 Offset values and larger hysteresis margins were selected to suppress ping-pong handovers and ensure stable connectivity. As the UE speed increases or RSRP degrades, the rules progressively reduce hysteresis and apply more aggressive A3 Offset values to enable earlier handover triggering.

This design ensures a smooth transition from stability-oriented behavior at low speed to responsiveness-oriented behavior at high speed. The FLC 2 rule base (Table III) enforces an inverse relationship between UE speed and TTT. Longer TTT values are selected at low speeds to enhance stability, whereas shorter TTT values are applied at high speeds to avoid delayed handovers. By isolating TTT control in a dedicated FLC, rule interpretability is preserved, and excessive rule coupling is avoided.

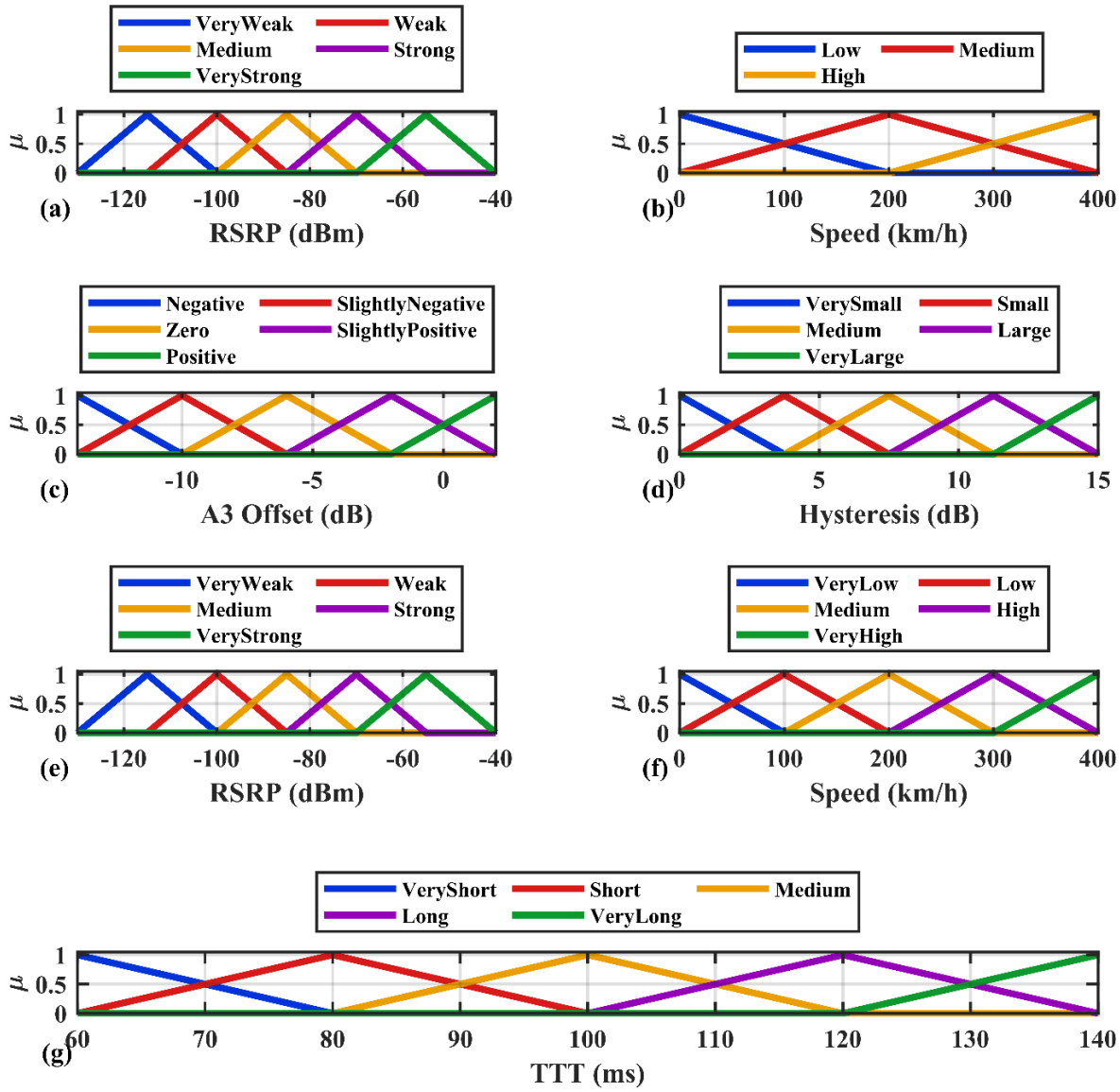

Fig. 5. Membership functions of the VADFLC input and output variables: (a) FLC 1 RSRP, (b) FLC 1 speed, (c) FLC 1 A3 Offset, (d) FLC 1 Hys, (e) FLC 2 RSRP, (f) FLC 2 speed, (g) FLC 2 TTT.

Figure 6 shows heat maps of the VADFLC fuzzy rules, illustrating the combined behavior of both rule bases and the joint adaptation of A3 Offset, hysteresis margin, and TTT with respect to UE speed and RSRP. As the speed increases, the controllers smoothly shift from conservative to aggressive handover control by assigning more negative A3 Offset values, reducing hysteresis margin, and shortening TTT; in contrast, the opposite behavior is maintained at low speeds to suppress unnecessary handovers. The continuous and well-structured control heat maps demonstrate that the handover parameters adapt smoothly to changing mobility conditions. This intelligent integration of speed and signal strength prevents abrupt and discontinuous handover transitions, which typically occur in basic threshold-based handover logic, thereby enhancing robustness in ultra-high-speed scenarios.

Both FLC segments employ Mamdani inference using Min–Max operators for rule evaluation and aggregation. Centroid defuzzification expressed in (13) [24] was applied to generate smooth and stable crisp outputs suitable for real-time handover adaptation:

$$x^* = \frac{\int_a^b \mu_A(x)\, x\, dx}{\int_a^b \mu_A(x)\, dx} \quad (13)$$

where x^* denotes the defuzzified value (crisp output) of fuzzy set A; $\mu_A(x)$ is the membership function of A, which gives the degree to which each sample x belongs to A; a and b denote the lower and upper bounds of the domain of x over which $\mu_A(x)$ is defined; x is the variable in the domain; and dx is the differential element of integration.

TABLE II. FLC 1 RULE BASE FOR A3 OFFSET AND HYSTERESIS OPTIMIZATION

RSRP	UE speed	A3 Offset	Hys
VeryWeak	Low	Positive	VeryLarge
Weak	Low	Positive	VeryLarge
Medium	Low	SlightlyPositive	Large
Strong	Low	SlightlyPositive	Large
VeryStrong	Low	SlightlyPositive	Large
VeryWeak	Medium	Zero	Medium
Weak	Medium	Zero	Medium
Medium	Medium	Zero	Medium
Strong	Medium	SlightlyNegative	Medium
VeryStrong	Medium	SlightlyNegative	Medium
VeryWeak	High	Negative	VerySmall
Weak	High	Negative	VerySmall
Medium	High	SlightlyNegative	Small
Strong	High	SlightlyNegative	Small

TABLE III. FLC 2 RULE BASE FOR TTT OPTIMIZATION

RSRP	UE speed	TTT
Any	VeryHigh	VeryShort
Any	High	Short
VeryWeak	Medium	Short
Weak	Medium	Short
Medium/Strong/VeryStrong	Medium	Medium
VeryWeak	Low	Medium
Weak	Low	Medium
Medium/Strong/VeryStrong	Low	Long
VeryWeak	VeryLow	Long
Weak	VeryLow	Long
Medium/Strong/VeryStrong	VeryLow	VeryLong

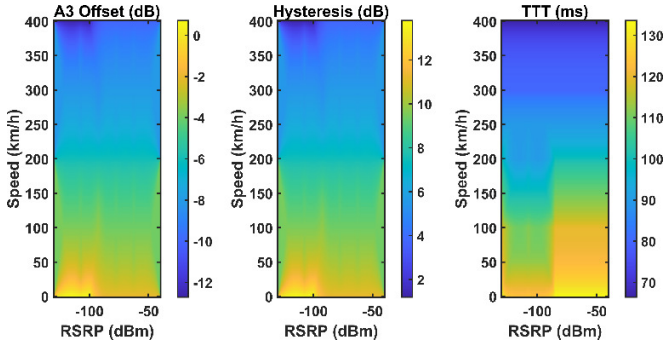

Fig. 6. Heat maps of VADFLC fuzzy rules for adaptive HCP optimization.

The updated A3 Offset, Hys, and TTT values were computed at each measurement instant and directly applied to the Event A3 HO triggering condition. The low complexity of the Mamdani inference and defuzzification procedures makes the real-time implementation of the proposed VADFLC feasible.

C. Simulation and Evaluation of Velocity-Adaptive Dual-Segment Fuzzy Logic Controller Framework

In the final step of the proposed methodology, the designed complete VADFLC framework was implemented in a MATLAB simulation environment to evaluate its performance in ultra-high-mobility 5G RMa scenarios. As illustrated in Figure 7, the 5G RMa setup (system and channel model) developed forms the basis of the simulation, wherein a single UE traverses a straight railway track at velocities of up to 400 km/h, and real-time measurements of the UE speed and serving cell RSRP were obtained. These measurements were fed into the designed dual-segment fuzzy logic controllers, wherein FLC 1 adaptively tunes the A3 Offset and Hys, whereas FLC 2 tunes the TTT. The defuzzified outputs of the fuzzy logic controllers were applied to the Event A3 HO triggering condition, which dynamically triggers handovers when the condition is satisfied. Performance metrics such as the Handover Rate (HOR), Handover Ping-Pong (HOPP) ratio, and HOD were monitored and logged during the simulation process to assess mobility robustness and handover efficiency. This final step of the methodology enabled a comprehensive analysis of the performance of the VADFLC framework in sustaining reliable connectivity in 5G high-speed scenarios.

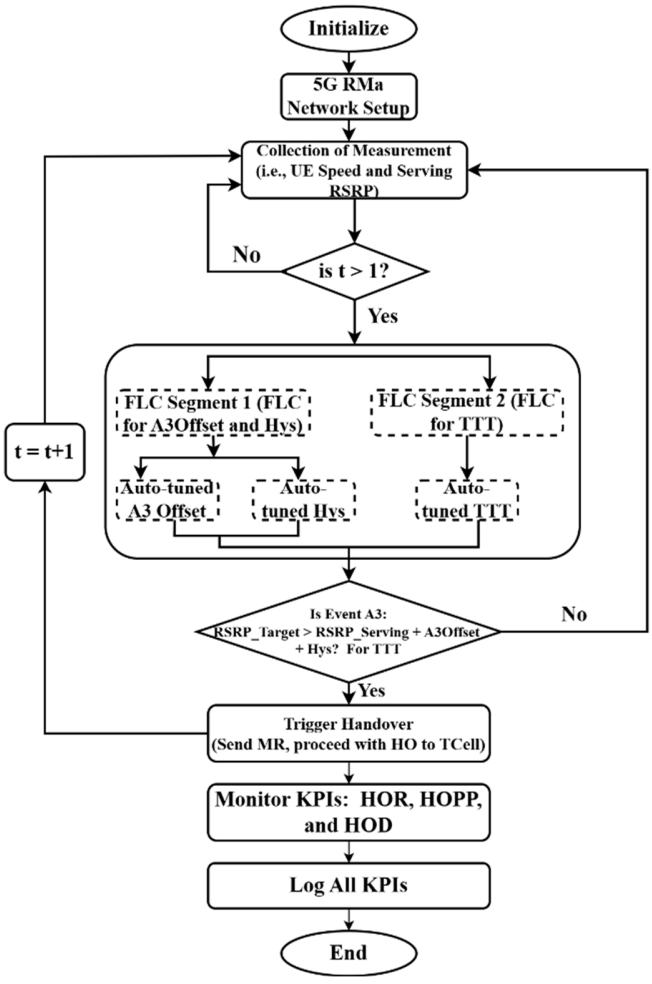

Fig. 7. Proposed VADFLC framework flow chart.

III. RESULTS AND DISCUSSION

This section discusses the simulation results obtained in this study. These results aim to verify the validity of the proposed framework in enhancing handover performance by dynamically tuning the three HCPs, namely, A3 Offset, Hys, and TTT, under ultra-high-mobility 5G RMa networks. The performance of the designed VADFLC was first evaluated by analyzing the optimized output values of A3 Offset, Hys, and TTT generated in response to real-time variations in the UE speed and RSRP. Then, the VADFLC framework performance was validated against the Traditional A3 algorithm, which employs fixed HCPs, using three key performance metrics: HOR, HOPP ratio, and HOD. Moreover, the approach proposed by authors in [20] was included as a benchmark to further support the generality and robustness of the proposed VADFLC approach.

A. Simulation Setup and Velocity-Adaptive Dual-Segment Fuzzy Logic Controller Evaluation

All simulations were performed using the MATLAB R2024b platform with the assistance of the Fuzzy Logic Toolbox, 5G Toolbox, Antenna Toolbox, and Communications Toolbox. The initial simulation parameters were configured to model a realistic HST scenario in a 5G RMa deployment. For all evaluated speed scenarios, a fixed trajectory length L of 100 km was used, whereas the simulation duration, T_{sim}, defined as $T_{sim} = L/v$, varied accordingly with the UE speed v to maintain consistent spatial coverage. Table IV summarizes the simulation parameters used in this study.

TABLE IV. SIMULATION PARAMETERS

Parameters	Values
Environment	RMa, Linear HST corridor
Inter-site distance (D)	5 km
Carrier frequency (f_c)	3.5 GHz
System bandwidth	100 MHz
BS transmit power	46 dBm / sector
gNodeB height	35 m
UE height (h_{UE})	3 m
Path-loss exponent (n)	2.1 (LoS), 3.0 (NLoS)
Shadow fading (σ)	6 dB (LoS), 8 dB (NLoS)
Noise spectral density	−174 dBm/Hz
Physical Resource Blocks (PRBs)	273
Subcarrier spacing	30 kHz
UE test speeds (v)	100–400 km/h
Mobility model	Linear uniform motion
Handover decision	Event A3 (RSRP-based)

Figure 8 shows the relationship between the RSRP of the serving cell and that of the strongest neighboring (target) cell, as received by the HST, against the train distance from the serving cell. It can be observed from the figure that, in the small-scale range depicted by the raw data, the signal fluctuates rapidly due to the combined effects of large-scale shadow fading, stochastic LoS/NLoS switching, and measurement noise. In the large-scale range depicted by the smoothed RSRP curves, a clear and physically consistent RSRP trend was observed: the serving cell RSRP level gradually decreased, whereas the strongest neighboring cell RSRP level gradually increased as the HST travelled from the serving cell towards the neighboring cell. This trend defines a realistic handover triggering region, located approximately between 1.40 km and 1.75 km from the serving cell, validating that the proposed system model can generate realistic handover-triggering conditions that conform to the Event A3 HO triggering criterion.

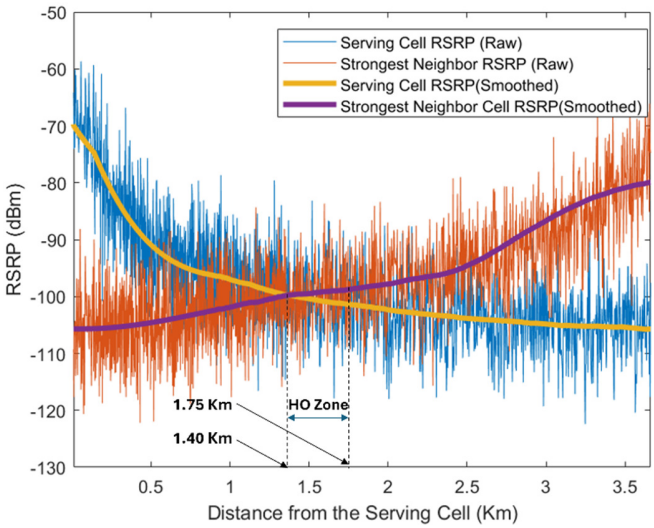

Fig. 8. RSRP of serving and neighboring cells versus HST distance from the serving cell.

Figure 9 depicts the average A3 Offset against train speed, illustrating the speed-dependent adaptation of the A3 Offset parameter from FLC 1 within the proposed VADFLC framework.

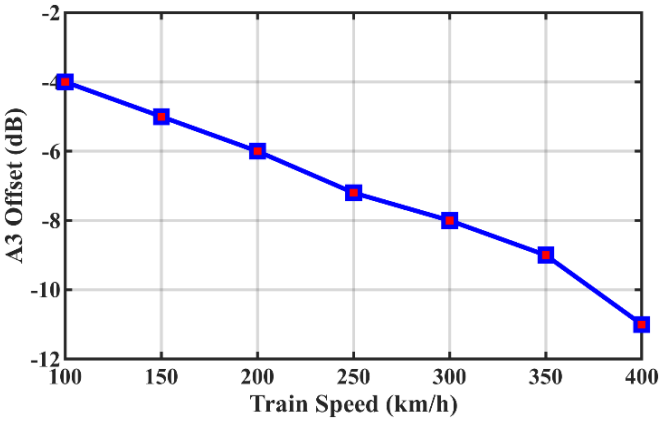

Fig. 9. Speed-dependent behavior of the A3 Offset parameter.

The A3 Offset decreases monotonically as the train speed increases. With an increasing train speed from 100 km/h to 400 km/h, the A3 Offset becomes increasingly negative, from approximately −4.0 dB to approximately −10.5 dB. This indicates that the proposed VADFLC reduces the neighbor cell dominance threshold at higher train speeds to trigger the handover earlier.

Such adaptation is particularly needed in high-mobility scenarios, where cell residence times are short; therefore, handovers must be triggered earlier to avoid excessive HOD. Additionally, the smooth and almost linear decreasing trend demonstrates that our FIS is capable of avoiding abrupt parameter changes and consequently preserves stable handover control.

Figure 10 shows the average hysteresis margin relative to train speed, illustrating the adaptation of the Hys parameter from FLC 1 within the proposed VADFLC framework. At lower speeds, it remains relatively high (approximately 9.0–9.5 dB at 100 km/h), which helps prevent unnecessary handovers and reduces the likelihood of HOPP caused by slow fading and shadowing. As the user speed increases, the hysteresis margin gradually decreases, reaching approximately 3 dB at 400 km/h.

This behavior reflects the intended VADFLC design, where stability is prioritized at low mobility, whereas responsiveness becomes important at high speeds, where excessive hysteresis could delay handovers and compromise connection reliability. This consistent downward trend demonstrates that the proposed VADFLC effectively balances the trade-off between handover stability and responsiveness across the full range of operating speeds.

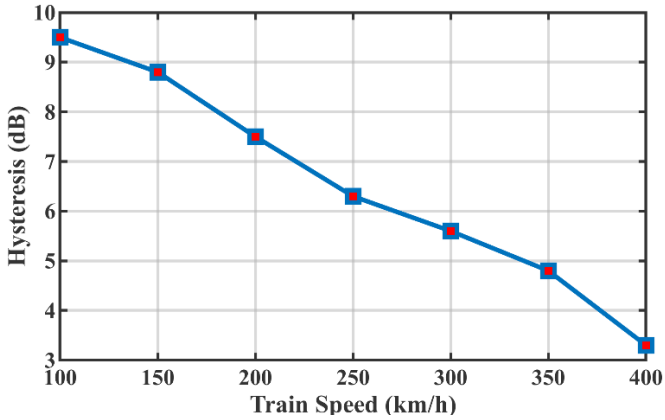

Fig. 10. Speed-dependent behavior of the hysteresis margin parameter.

Figure 11 depicts the average TTT against train speed, illustrating the inverse relationship between the TTT values produced by FLC 2 within the proposed VADFLC framework and train speed. At 100 km/h, the TTT is approximately 115 ms, allowing sufficient time for the Event A3 HO triggering condition to be satisfied and ensuring stable handover decisions. As the train speed increased, the TTT progressively reduced, reaching approximately 66 ms at 400 km/h.

This adaptation ensures that handover decisions are executed more rapidly at higher speeds, which is critical for maintaining seamless connectivity when the train traverses the cell coverage regions quickly. The smooth decline across all speed samples indicates that the train speed is prioritized as the dominant input for TTT control, as expected in the VADFLC design.

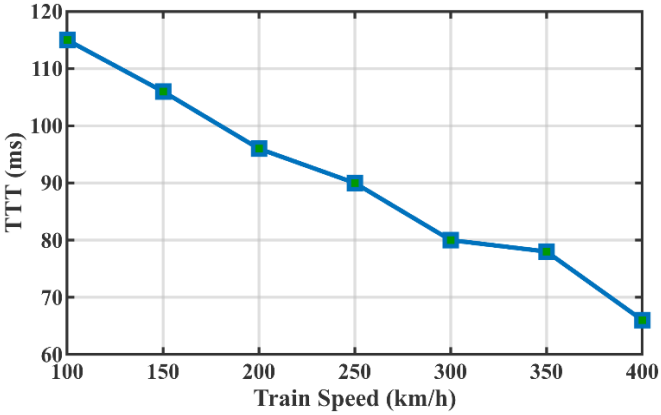

Fig. 11. Speed-dependent behavior of the TTT parameter.

B. Performance Metrics

1) Handover Rate

HOR quantifies the number of handovers performed by a UE during a given period (i.e., per second or per hour), as expressed in (14):

$$\mathrm{HOR} = \frac{N_{HO}}{T_{unit}} \quad (14)$$

where N_{HO} represents the total number of handovers executed during the observation period, and T_{unit} is the unit time interval over which the HOR is measured. In this study, for each algorithm, a handover was recorded when the Event A3 HO condition was satisfied and the TTT (ms) expired, resulting in a serving cell change.

Figure 12 compares the HOR between the proposed VADFLC and Traditional A3 algorithms for all test speeds (100-400 km/h). With a fixed inter-site distance D, and fixed-length trajectory L, increasing speed reduces the time required for the UE to traverse the trajectory, resulting in a higher number of cells crossed per unit time. This explains the observed increase in HOR with speed for both algorithms.

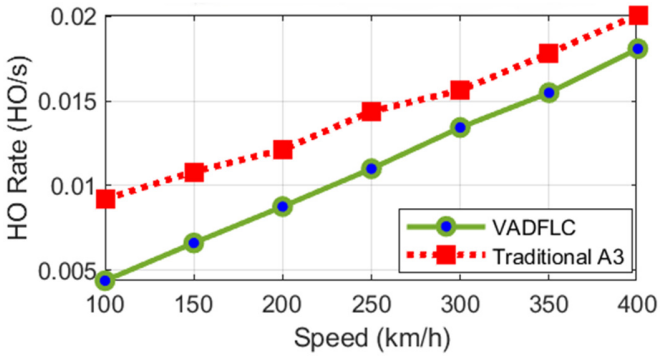

Fig. 12. HOR versus UE speed.

Further observations show that the HOR values for the proposed VADFLC framework are significantly lower than those of the Traditional A3 algorithm because the handover decision of the VADFLC continuously adapts with the speed and dynamically changing RSRP, thereby filtering out

unnecessary handovers that would result in a high HOR compared to the Traditional A3 algorithm. A high HOR increases the risk of higher signaling overhead, delayed handovers, and ping-pong handovers. In terms of the control-plane requirement, a lower HOR indicates lower control-plane signaling overhead and a lower probability of handover failure, which is highly desirable for HSTs, where seamless communication for safe operation requires minimal signaling congestion and fast, stable handover procedures.

2) Handover Ping-Pong Ratio

The HOPP ratio is a measure of the probability that a UE is handed back and forth between two adjacent cells in a short period of time. In this study, for each algorithm, the ping-pong events were identified from the serving cell history as transitions of the form cell $i \rightarrow j \rightarrow i$ within a short time window of 1 s. The HOPP ratio was computed using (15):

$$\mathrm{HOPP_{ratio}} = \frac{\mathrm{N_{HOPP}}}{\mathrm{N_{HOt}}} \quad (15)$$

where $\mathrm{N_{HOPP}}$ denotes the total number of ping-pong handover events detected during the observation period and $\mathrm{N_{HOt}}$ is the total number of handovers executed during the same observation period.

Figure 13 compares the HOPP ratio between the proposed VADFLC method and the Traditional A3 algorithm for all test speeds (100–400 km/h). The results demonstrate that the VADFLC achieves a substantially lower HOPP ratio across all speeds, indicating improved handover stability. As the UE speed increases, the dwell time in the overlapping coverage regime decreases, which in turn reduces the probability of repeated oscillations, thereby reducing the HOPP ratio. This predictable trend is evident in the Traditional A3 algorithm. Nonetheless, because of the static choice of the HCPs (Hys, A3 Offset, and TTT) that are not optimized in real time to accommodate the changes in user mobility, the Traditional A3 algorithm continues to have a considerably higher HOPP ratio than VADFLC throughout the speed range.

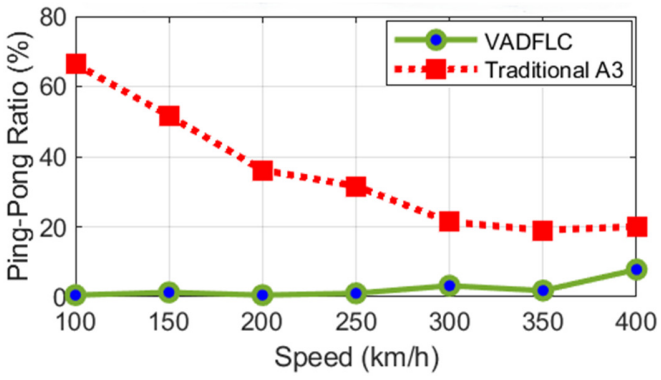

Fig. 13. HOPP ratio versus UE speed.

In contrast, the proposed VADFLC can adapt these HCPs based on the UE speed and serving cell signal level. Specifically, the adaptive Hys and A3 Offset generated by FLC 1 create a velocity-adaptive and signal-dependent switching margin that is sufficiently large at low speeds to mitigate oscillatory behavior and sufficiently small at high speeds to enable stable handover adaptation. As a result, the proposed VADFLC significantly reduces the HOPP ratio, achieving reductions of up to 95% at low speeds and maintaining improvements above 50% even at high speeds compared to the Traditional A3 algorithm.

3) Handover Delay

HOD is defined as the time required to complete a handover once the handover triggering condition is satisfied. In this study, for each algorithm, the HOD was measured as the interval between the moment a handover was initiated and the instant at which the UE successfully established a connection with the target cell. It includes both a configured TTT and the processing and signaling delays required to execute a handover. Only successful handovers were considered in the computation of the HOD to ensure that the metric accurately reflects mobility execution rather than failed handovers. The average HOD ($\mathrm{HOD_{avg}}$) was calculated by averaging the delays of all successful handovers during the simulation time, as expressed in (16):

$$\mathrm{HOD_{avg}} = \frac{1}{\mathrm{N}}\sum_{\mathrm{n=1}}^{\mathrm{N}} \Delta \mathrm{t_{HO}^{(n)}}, \quad \Delta \mathrm{t_{HO}^{(n)}} = \mathrm{t_c^{(n)}} - \mathrm{t_t^{(n)}} \quad (16)$$

where N is the total number of successful handovers, $\Delta \mathrm{t_{HO}^{(n)}}$ represents the HOD for the $\mathrm{n^{th}}$ successful handover, $\mathrm{t_c^{(n)}}$ is the time at which the $\mathrm{n^{th}}$ handover is completed, and $\mathrm{t_t^{(n)}}$ is the time at which the $\mathrm{n^{th}}$ handover is triggered.

Figure 14 shows the average HOD for the VADFLC and the Traditional A3 algorithms against UE speed. The results indicate that the HOD of the VADFLC decreases with increasing speed, whereas the baseline maintains an almost constant delay. Specifically, the delay reduces from approximately 130 ms at 100 km/h to about 87 ms at 400 km/h, corresponding to an approximate 33% reduction across the evaluated speed range. Although the proposed VADFLC exhibits higher HOD at low-to-moderate speeds, it converges to the Traditional A3 algorithm at higher speeds, indicating comparable delay performance under high-mobility conditions.

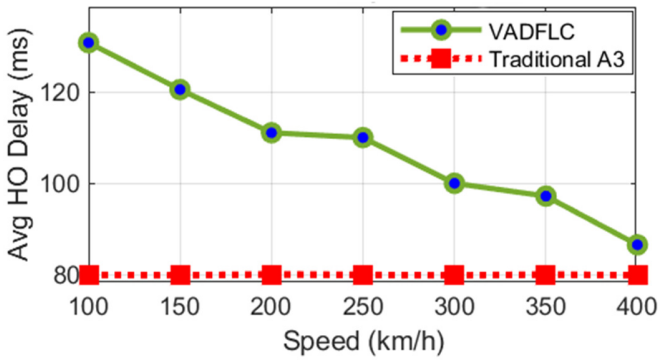

Fig. 14. HOD versus UE speed.

The trend of the observed HOD is attributed to velocity-adaptive TTT selection in the proposed VADFLC. At low speeds, a larger TTT is selected to ensure handover stability

and reduce unnecessary triggering, which increases delay. As the UE speed increases, the controller reduces TTT to enable faster handover execution and avoid late triggering. In contrast, the Traditional A3 algorithm uses fixed HCPs, resulting in lower delay at low speeds but limited adaptability to increasing UE speeds.

To further validate the generality of the proposed VADFLC framework, an additional set of experiments was performed using the simulation framework and channel model proposed by authors in [20] for 5G-R. This framework simulates a one-dimensional rail corridor with equally spaced BSs separated by a distance d_{bs} of 2.5 km. It employs the COST231-Hata large-scale path loss with log-normal shadowing σ of 6 dB and computes the per-link Signal-to-Interference-plus-Noise Ratio (SINR) by treating all other BSs as interferers. Fifty Monte Carlo trials of a 60 s run were conducted for each speed from 100 to 350 km/h, using a time step of 0.1 s. Three algorithms were compared under the same realizations: A Traditional A3 algorithm with a fixed hysteresis margin of 3 dB, a 5G-R hierarchical fuzzy controller, and the proposed VADFLC framework that uses the same dual-segment FIS models for adapting A3 Offset, Hys, and TTT HCPs.

The observations of the test are illustrated in Figure 15, where we observe that the Traditional A3 algorithm has an overall mean delay of 116.3 ms. This delay remains almost unchanged as UE speed increases because the handover decision is governed by fixed HCPs. Consequently, the algorithm lacks the flexibility to adapt its triggering behavior to different UE speeds and channel conditions.

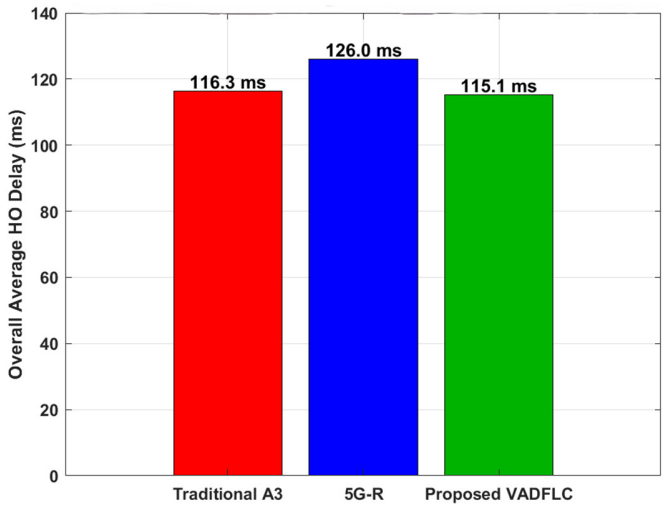

Fig. 15. Comparison of average HOD for three algorithms.

Compared with the Traditional A3 algorithm, our VADFLC framework has the lowest overall mean of 115.1 ms, corresponding to an absolute improvement of 1.2 ms (~1.0% gain compared with Traditional A3). This modest but consistent reduction is aligned with the speed-aware adaptation of the controller, which lowers the effective handover triggering time at high mobility to sustain timely execution. In contrast, the 5G-R hierarchical fuzzy framework has the highest overall mean delay of 126.0 ms, which is 9.7 ms (~8.3%) higher than that of the Traditional A3 algorithm.

Overall, the additional evaluation of the 5G-R simulation framework further validates the robustness and generality of the proposed VADFLC approach. VADFLC outperformed the other schemes in terms of having the lowest mean HOD, even under a different channel model and handover evaluation setup. This demonstrates that the proposed VADFLC scheme can perform well under heterogeneous modeling conditions, highlighting its suitability for ultra-high-mobility 5G scenarios such as HSTs.

IV. CONCLUSION

This study proposes a Velocity-Adaptive Dual-Segment Fuzzy Logic Controller (VADFLC) for optimizing key Handover Control Parameters (HCPs), namely hysteresis margin, A3 Offset, and Time-to-Trigger (TTT), in ultra-high mobility fifth-generation (5G) networks based on User Equipment (UE) speed and serving cell Reference Signal Received Power (RSRP). The novelty of this study lies in the joint and coordinated optimization of these three HCPs within a dual segment fuzzy logic architecture, together with its effectiveness under ultra-high mobility conditions characterized by rapid variations in UE speed and channel quality.

Simulation results under the Rural Macrocell (RMa) scenario show that the proposed VADFLC framework achieves an average Handover Rate (HOR) reduction of approximately 25.5% compared to the Traditional A3 algorithm, thereby reducing unnecessary handovers and lowering the Handover Ping-Pong (HOPP) ratio to nearly zero at certain UE speeds. In addition, the proposed approach reduces Handover Delay (HOD), particularly at high UE speeds, and improves overall handover stability and execution timeliness in demanding scenarios such as High-Speed Train (HST) environments.

Despite its effectiveness, the proposed VADFLC requires expert tuning, precise data, and further validation under more diverse real-world scenarios beyond the conditions considered in this study. Hence, future work will consider utilizing predictive data-driven methods, such as Long Short-Term Memory (LSTM), reinforcement learning, and Adaptive Neuro-Fuzzy Inference System (ANFIS), to improve the robustness of the proposed VADFLC framework. Furthermore, key performance metrics such as Handover Failure (HOF) and Radio Link Failure (RLF) will be considered to extend this study.

DECLARATION OF COMPETING INTERESTS

The authors declare that they have no known conflict of interests.

ACKNOWLEDGMENT

The authors would like to thank the African Union and the African Union Commission for their commitment to promoting scientific research and technological innovation in Africa. This study was supported by the Pan African University Institute for Basic Sciences, Technology, and Innovation through funding and institutional support.

DATA AVAILABILITY

The data that support the findings of this study are available within this article.

DECLARATION OF GENERATIVE AI USE

The authors declare that they did not use any generative AI tools in the preparation of this manuscript.

REFERENCES

[1] F. Hasegawa *et al.*, "High-Speed Train Communications Standardization in 3GPP 5G NR," *IEEE Communications Standards Magazine*, vol. 2, no. 1, pp. 44–52, Mar. 2018, https://doi.org/10.1109/MCOMSTD.2018.1700064.

[2] J. G. Andrews *et al.*, "What Will 5G Be?," *IEEE Journal on Selected Areas in Communications*, vol. 32, no. 6, pp. 1065–1082, June 2014, https://doi.org/10.1109/JSAC.2014.2328098.

[3] R. He *et al.*, "5G for Railways: Next Generation Railway Dedicated Communications," *IEEE Communications Magazine*, vol. 60, no. 12, pp. 130–136, Dec. 2022, https://doi.org/10.1109/MCOM.005.2200328.

[4] *5G; Study on channel model for frequencies from 0.5 to 100 GHz*, 3GPP TR 38.901 version 18.0.0 Release 18, 3rd Generation Partnership Project (3GPP), Valbonne, France, 2024.

[5] A. I. Mbulwa, H. T. Yew, A. Chekima, and J. A. Dargham, "Self-Optimization of Handover Control Parameters for 5G Wireless Networks and Beyond," *IEEE Access*, vol. 12, pp. 6117–6135, 2024, https://doi.org/10.1109/ACCESS.2023.3346039.

[6] E. Gures, I. Shayea, A. Alhammadi, M. Ergen, and H. Mohamad, "A Comprehensive Survey on Mobility Management in 5G Heterogeneous Networks: Architectures, Challenges and Solutions," *IEEE Access*, vol. 8, pp. 195883–195913, 2020, https://doi.org/10.1109/ACCESS.2020.3030762.

[7] B. Duan, C. Li, J. Xie, W. Wu, and D. Zhou, "Fast Handover Algorithm Based on Location and Weight in 5G-R Wireless Communications for High-Speed Railways," *Sensors*, vol. 21, no. 9, Apr. 2021, Art. no. 3100, https://doi.org/10.3390/s21093100.

[8] W. K. Saad, I. Shayea, B. J. Hamza, A. Azizan, M. Ergen, and A. Alhammadi, "Performance Evaluation of Mobility Robustness Optimization (MRO) in 5G Network With Various Mobility Speed Scenarios," *IEEE Access*, vol. 10, pp. 60955–60971, 2022, https://doi.org/10.1109/ACCESS.2022.3173255.

[9] A. a. M. K. Abuelgasim and K. M. Yusof, "High Speed Mobility Management Performance in a Real LTE Scenario," *Engineering, Technology & Applied Science Research*, vol. 10, no. 1, pp. 5175–5179, Feb. 2020, https://doi.org/10.48084/etasr.3245.

[10] *5G; NR; Radio Resource Control (RRC); Protocol specification*, 3GPP TS 38.331 version 18.1.0 Release 18, 3rd Generation Partnership Project (3GPP), Valbonne, France, 2024.

[11] P. Muñoz, R. Barco, and I. de la Bandera, "On the Potential of Handover Parameter Optimization for Self-Organizing Networks," *IEEE Transactions on Vehicular Technology*, vol. 62, no. 5, pp. 1895–1905, June 2013, https://doi.org/10.1109/TVT.2013.2247778.

[12] M. Manalastas, M. U. B. Farooq, S. M. A. Zaidi, A. Abu-Dayya, and A. Imran, "A Data-Driven Framework for Inter-Frequency Handover Failure Prediction and Mitigation," *IEEE Transactions on Vehicular Technology*, vol. 71, no. 6, pp. 6158–6172, June 2022, https://doi.org/10.1109/TVT.2022.3157802.

[13] A. Alhammadi, M. Roslee, M. Y. Alias, I. Shayea, S. Alraih, and K. S. Mohamed, "Auto Tuning Self-Optimization Algorithm for Mobility Management in LTE-A and 5G HetNets," *IEEE Access*, vol. 8, pp. 294–304, 2020, https://doi.org/10.1109/ACCESS.2019.2961186.

[14] M. T. Nguyen, S. Kwon, and H. Kim, "Mobility Robustness Optimization for Handover Failure Reduction in LTE Small-Cell Networks," *IEEE Transactions on Vehicular Technology*, vol. 67, no. 5, pp. 4672–4676, May 2018, https://doi.org/10.1109/TVT.2017.2787602.

[15] Y. S. Hussein, B. M. Ali, M. F. A. Rasid, A. Sali, and A. M. Mansoor, "A novel cell-selection optimization handover for long-term evolution (LTE) macrocellusing fuzzy TOPSIS," *Computer Communications*, vol. 73, pp. 22–33, Jan. 2016, https://doi.org/10.1016/j.comcom.2015.10.001.

[16] S. Alraih, R. Nordin, A. Abu-Samah, I. Shayea, N. F. Abdullah, and A. Alhammadi, "Robust Handover Optimization Technique with Fuzzy Logic Controller for Beyond 5G Mobile Networks," *Sensors*, vol. 22, no. 16, Aug. 2022, Art. no. 6199, https://doi.org/10.3390/s22166199.

[17] W.-S. Hwang, T.-Y. Cheng, Y.-J. Wu, and M.-H. Cheng, "Adaptive Handover Decision Using Fuzzy Logic for 5G Ultra-Dense Networks," *Electronics*, vol. 11, no. 20, Oct. 2022, Art. no. 3278, https://doi.org/10.3390/electronics11203278.

[18] H. Riaz, S. Öztürk, and A. Çalhan, "A Robust Handover Optimization Based on Velocity-Aware Fuzzy Logic in 5G Ultra-Dense Small Cell HetNets," *Electronics*, vol. 13, no. 17, Aug. 2024, Art. no. 3349, https://doi.org/10.3390/electronics13173349.

[19] A. Alhammadi, M. Roslee, M. Y. Alias, I. Shayea, and A. Alquhali, "Velocity-Aware Handover Self-Optimization Management for Next Generation Networks," *Applied Sciences*, vol. 10, no. 4, Feb. 2020, Art. no. 1354, https://doi.org/10.3390/app10041354.

[20] B. Zhu and X. Li, "Research on 5G-R Handover Algorithm with Improved Fuzzy Logic," in *2024 6th International Conference on Communications, Information System and Computer Engineering*, Guangzhou, China, 2024, pp. 766–769, https://doi.org/10.1109/CISCE62493.2024.10653032.

[21] M. L. Marí-Altozano, S. S. Mwanje, S. L. Ramírez, M. Toril, H. Sanneck, and C. Gijón, "A Service-Centric Q-Learning Algorithm for Mobility Robustness Optimization in LTE," *IEEE Transactions on Network and Service Management*, vol. 18, no. 3, pp. 3541–3555, Sept. 2021, https://doi.org/10.1109/TNSM.2021.3073244.

[22] H. Riaz, S. Öztürk, S. Aldirmaz-Colak, and A. Çalhan, "A Handover Decision Optimization Method Based on Data-Driven MLP in 5G Ultra-Dense Small Cell HetNets," *Journal of Network and Systems Management*, vol. 33, no. 2, Feb. 2025, Art. no. 31, https://doi.org/10.1007/s10922-025-09903-6.

[23] S. Sun *et al.*, "Investigation of Prediction Accuracy, Sensitivity, and Parameter Stability of Large-Scale Propagation Path Loss Models for 5G Wireless Communications," *IEEE Transactions on Vehicular Technology*, vol. 65, no. 5, pp. 2843–2860, May 2016, https://doi.org/10.1109/TVT.2016.2543139.

[24] T. J. Ross, *Fuzzy Logic With Engineering Applications*, 3rd ed. Hoboken, NJ, USA: Willey, 2010, https://doi.org/10.1002/9781119994374.